processes

MDPI

Article

Efficiency of Hydrogen Peroxide and Fenton Reagent for Polycyclic Aromatic Hydrocarbon Degradation in Contaminated Soil: Insights from Experimental and Predictive Modeling

Mahdia Smara [1], Razika Khalladi [1], Nadji Moulai-Mostefa [1], Kamilia Madi [2], Dorsaf Mansour [3], Sabrina Lekmine [4], Ouided Benslama [5], Hichem Tahraoui [2,6], Jie Zhang [7] and Abdeltif Amrane [6,*]

1 Materials and Environment Laboratory (LME), Department of Process Engineering and Environment, Faculty of Technologie, Yahia Fares University, Medea 26000, Algeria; smaramahdia@outlook.fr (M.S.); r_khalladi@yahoo.fr (R.K.); moulai_nadji@yahoo.fr (N.M.-M.)
2 Laboratoire de Génie des Procédés Chimiques, Department of Process Engineering, University of Ferhat Abbas, Setif 19000, Algeria; madikamilia1998@gmail.com (K.M.); hichemm.tahraouii@gmail.com (H.T.)
3 Chemistry Department, College of Sciences, University of Ha'il, Hail 2440, Saudi Arabia; mansour_dorsaf@yahoo.fr
4 Biotechnology, Water, Environment and Health Laboratory, Abbes Laghrour University, Khenchela 40004, Algeria; lekmine.sabrina@univ-khenchela.dz
5 Laboratory of Natural Substances, Biomolecules and Biotechnological Applications, Department of Natural and Life Sciences, Larbi Ben M'Hidi University, Oum El Bouaghi 04000, Algeria; benslama.wided@hotmail.fr
6 Univ Rennes, Ecole Nationale Supérieure de Chimie de Rennes, CNRS, ISCR—UMR6226, 35000 Rennes, France
7 School of Engineering, Merz Court, Newcastle University, Newcastle upon Tyne NE1 7RU, UK; jie.zhang@newcastle.ac.uk
* Correspondence: abdeltif.amrane@univ-rennes.fr

Abstract: This study investigates the degradation kinetics of polycyclic aromatic hydrocarbons (PAHs) in contaminated soil using hydrogen peroxide (H_2O_2) and the Fenton process (H_2O_2/Fe^{2+}). The effect of oxidant concentration and the Fenton molar ratio on PAH decomposition efficiency is examined. Results reveal that increasing H_2O_2 concentration above 25 mmol/samples leads to a slight increase in the rate constants for both first- and second-order reactions. The Fenton process demonstrates higher efficiency in PAH degradation compared to H_2O_2 alone, achieving decomposition yields ranging from 84.7% to 99.9%. pH evolution during the oxidation process influences PAH degradation, with alkaline conditions favoring lower elimination rates. Fourier-transform infrared (FTIR) spectroscopy analysis indicates significant elimination of PAHs after treatment, with both oxidants showing comparable efficacy in complete hydrocarbon degradation. The mechanisms of PAH degradation by H_2O_2 and the Fenton process involve hydroxyl radical formation, with the latter exhibiting greater efficiency due to Fe^{2+} catalysis. Gaussian process regression (GPR) modeling accurately predicts reduced concentration, with optimized ARD-Exponential kernel function demonstrating superior performance. The Improved Grey Wolf Optimizer algorithm facilitates optimization of reaction conditions, yielding a high degree of agreement between experimental and predicted values. A MATLAB 2022b interface is developed for efficient optimization and prediction of C/C_0, a critical parameter in PAH degradation studies. This integrated approach offers insights into optimizing the efficiency of oxidant-based PAH remediation techniques, with potential applications in contaminated soil remediation.

Keywords: soil pollution; polycyclic aromatic hydrocarbons; hydrogen peroxide; the Fenton reagent; chemical oxidation; Gaussian process regression; Improved Grey Wolf Optimizer

Citation: Smara, M.; Khalladi, R.; Moulai-Mostefa, N.; Madi, K.; Mansour, D.; Lekmine, S.; Benslama, O.; Tahraoui, H.; Zhang, J.; Amrane, A. Efficiency of Hydrogen Peroxide and Fenton Reagent for Polycyclic Aromatic Hydrocarbon Degradation in Contaminated Soil: Insights from Experimental and Predictive Modeling. *Processes* **2024**, *12*, 621. https://doi.org/10.3390/pr12030621

Academic Editor: Guining Lu

Received: 29 February 2024
Revised: 18 March 2024
Accepted: 19 March 2024
Published: 21 March 2024

1. Introduction

Polyaromatic hydrocarbons (PAHs) represent a pervasive environmental challenge, ubiquitous in their occurrence and formidable in their impact. Originating primarily from the incomplete combustion of diverse organic materials such as coal, petroleum, gasoline, and wood, these compounds have earned their place as high-priority pollutants. The urgency surrounding PAHs is fueled by their marked toxicity, carcinogenicity, teratogenicity, and a remarkable resistance to degradation [1]. Their ability to exhibit low water solubility and exceptional chemical stability perpetuates their presence in soil, creating lasting repercussions for both ecosystems and human health [2]. As industrial activities significantly contribute to soil pollution, the imperative for effective and sustainable soil remediation strategies becomes increasingly apparent [3,4]. The classification of PAHs as persistent organic pollutants (POPs) underscores the magnitude of the challenge, necessitating comprehensive, ecologically sound, cost-effective, and efficient soil restoration approaches [5]. The intricate interplay between PAHs and soil further complicates the remediation landscape. These compounds exhibit sequestration and strong sorption tendencies to soil organic matter, rendering them less accessible and posing a formidable challenge to traditional treatment methodologies such as biological processes, soil extraction, or washing. In response, the avenue of chemical oxidation emerges as a promising and dynamic solution, presenting opportunities for targeted and effective pollutant degradation. Success in this endeavor hinges on a nuanced understanding of soil properties, contaminant levels, and specific remediation objectives, recognizing that the efficiency of these methods is contingent upon the effective interaction between oxidants and contaminants [6,7]. Within this context, mixed chemical oxidation, characterized by the sequential combination of surfactants and oxidants, has demonstrated noteworthy success in removing PAHs from contaminated soils, showcasing robust remediation efficiency across diverse soil particles and pollution levels [8,9]. Extensive work has been devoted to developing soil remediation techniques [10], which mainly involves physical, chemical, and biological processes or/and their combinations. Advanced oxidation processes (AOPs) are powerful chemical methods with growing popularity for organic-contaminated soil remediation, being considered more effective than physical and biological approaches [11]. The process of chemical oxidation, involving the injection of an oxidant solution into the treatment zone, serves as a transformative tool, particularly in soils burdened by a historical legacy of contamination by toxic and persistent organic pollutants [12,13]. In this intricate landscape, hydrogen peroxide (H_2O_2) and hydrogen peroxide via the Fenton reaction emerge as key oxidants. One of the most frequently AOPs used is the Fenton process ($H_2O_2 + Fe^{2+}$), where H_2O_2 is the oxidant species and homogeneous Fe(II) acts as a catalyst for hydrogen peroxide decomposition [14,15], each with its unique characteristics and applications. While the application of hydrogen peroxide is tempered by its limitations under neutral pH conditions due to the formation of water, the Fenton reaction provides a pathway marked by high reactivity of the hydroxyl radical (OH), capable of oxidizing a diverse array of organic contaminants, facilitated by an alkaline pH in the chemical reaction [14,16]. The research into the chemical oxidation of PAHs, often conducted at the laboratory scale in stirred closed reactors, offers valuable insights. Frequently utilizing samples from industrially contaminated areas marked by petroleum activity, these studies investigate the effects of chosen oxidants, providing a foundation for a deeper understanding of the intricate dynamics involved in pollutant removal [17,18]. The careful selection of oxidants in such studies is guided not only by their effectiveness but also by the imperative to preserve the integrity of the soil environment. Noteworthy observations, such as the influence of Fenton reagent on total organic carbon (TOC) content in the soil and its impact on indigenous soil microbe growth, contribute key insights into enhancing PAH remediation strategies and evaluating their ecological implications [19]. As concerns surrounding the environmental impact of rapid petroleum hydrocarbon degradation through chemical oxidation continue to grow, the quest for environmentally friendly activation methods gains prominence [20]. Against this backdrop, this study sets out with the overarching objective of comprehen-

sively assessing the efficiency of chemical oxidation. It aims to unravel the multifaceted impact of this remediation strategy on PAH content, availability, structure, and crucial soil properties, such as organic matter content and pH. Through meticulous treatment of eight contrasting samples of contaminated soil, coupled with a stringent control of pH and temperature, the study seeks to contribute to the evolving understanding of environmentally conscious approaches to soil remediation. The chosen oxidants, hydrogen peroxide and a modified Fenton reagent, serve as focal points in exploring the delicate balance between effectiveness and environmental preservation [21]. In essence, this investigation endeavors to navigate the complexities of PAH remediation, advancing our understanding of chemical oxidation as a potent tool in the pursuit of a sustainable and ecologically responsible remediation strategy. In this research, a comprehensive exploration of polycyclic aromatic hydrocarbons (PAHs) degradation was conducted through chemical oxidation processes using hydrogen peroxide (H_2O_2) and the Fenton method (H_2O_2/Fe^{2+}). The experiments investigated the impact of oxidant concentration and the H_2O_2/Fenton molar ratio on the kinetics of PAH decomposition, while also monitoring pH evolution during oxidation. A comparative analysis of degradation results revealed significantly higher efficiency of the Fenton method compared to isolated H_2O_2. Additionally, an examination of degradation mechanisms elucidated the underlying chemical reactions involved in PAH decomposition. Concurrently, Gaussian process regression (GPR) modeling was employed to optimize degradation conditions, integrating the Improved Grey Wolf Optimizer (IGWO) algorithm to determine optimal settings. Finally, an optimization and prediction interface were developed using MATLAB, aimed at minimizing the reduced concentration ratio (C/C_0), a critical parameter of the study, through IGWO. This interface allows researchers and practitioners to input necessary parameters for optimization, providing precise and reliable results based on the GPR model. This work collectively represents a crucial contribution to the development of effective remediation strategies against PAH contamination in soils, underscoring the importance of predictive modeling in environmental management. The novelty of this work lies in several aspects. Firstly, it provides a comprehensive investigation into the degradation of polycyclic aromatic hydrocarbons (PAHs) using both hydrogen peroxide (H_2O_2) and the Fenton process (H_2O_2/Fe^{2+}), considering factors such as oxidant concentration and the H_2O_2/Fenton molar ratio. This holistic approach contributes to a deeper understanding of the degradation kinetics and mechanisms involved. Secondly, the integration of Gaussian process regression (GPR) modeling, coupled with the Improved Grey Wolf Optimizer (IGWO) algorithm, for optimizing degradation conditions represents an innovative methodological approach. This combination allows for the identification of optimal degradation settings, enhancing the efficiency and effectiveness of the remediation process. Furthermore, the development of an optimization and prediction interface using MATLAB adds practical value to the research. This interface facilitates the input of parameters for optimization and provides accurate predictions based on the GPR model, offering a user-friendly tool for researchers and practitioners in the field of environmental management. Overall, the novelty of this work lies in its integrated approach, combining experimental investigations, advanced modeling techniques, and practical application development to address the challenge of PAH contamination in soils.

2. Materials and Methods

2.1. Reagents

The chemicals used are hydrogen peroxide (H_2O_2, 50%), and ferrous sulfate heptahydrate ($FeSO_4 \cdot 7H_2O$, 84%). All products were supplied by Sigma Aldrich, Saint-Louis, MO, USA.

2.2. Contaminated Soil Sampling and Preparation of Samples

Sampling activities were meticulously carried out at a refinery station situated in the GL1-Z zone in Arzew (Oran), western Algeria, where the environment has been significantly impacted by a year-long presence of petroleum activities, resulting in contamination

with polycyclic aromatic hydrocarbons (PAHs). The collection of soil samples was a thorough process, encompassing depths from 0 m to 2.9 m. Post-collection, the samples underwent a series of meticulous procedures, including air-drying at room temperature, sieving to a granularity of 0.8 mm, and homogenization utilizing the quartering method (performed twice). These steps were undertaken to derive a representative sample, denoted as PS, which encapsulates the characteristics of the polluted soil. Subsequently, the PS sample was conscientiously stored at 4 °C in a dark environment, ensuring the preservation of its integrity until future analysis [22].

The analytical results for the collected soil samples provided insights into their composition, revealing a distinctive silty–sandy texture. These findings, crucial for understanding the soil's characteristics, are comprehensively detailed in Table 1.

Table 1. Properties of the contaminated soil.

Texture	pH	Electric Conductivity (mS/m)	Organic Matter (%)	Humidity	Density (g/cm^3)
Sand 40% Silt 48% Clay 12%	7.05	8.06	6.0	0.12	2.60

The extraction process involved drawing the upper organic phase (ranging from 10 to 25 mL) using a liquid-phase microinjector, followed by meticulous dilution to 1.0 mL with n-hexane in preparation for gas chromatography–mass spectrometry (GC-MS) analysis. To ensure precision, all degradation experiments mentioned earlier were conducted with careful repetition, totaling three iterations. After employing acetonitrile for solvent extraction of the sorbed polycyclic aromatic hydrocarbons (PAHs), the quantification of these compounds was performed utilizing a GC-MS system (Shimadzu). This system featured a diode array UV detector, a Prosphere C-18 column (Alltech, 250 mm × 46 mm, particle size 5 μm), and a pre-column (Alltech, 150 mm × 4.6 mm).

The mobile phase comprised an 85% mixture of acetonitrile and 15% ultrapure water, with a flow rate set at 0.4 mL min^{-1}. External calibrations were performed using a standard mixture of 16 PAHs from the US Environmental Protection Agency (USEPA) in acetonitrile within the 1–100 mg/L range (Dr. Ehrenstorfer PAH-Mix 9) with five calibration levels. Five calibration levels were employed to ensure accuracy in the calibration process. The detailed and comprehensive results stemming from these analyses are methodically presented in Table 2.

Table 2. Composition of polluted soil.

	Elements	Concentration (mg/kg Soil)	Elements	Concentration (mg/kg Soil)
BTEX	Benzene	<0.01		
	Ethylbenzene	<0.01		
	Styrene	<0.01		
	Toluene	0.001		
	Xylene	0.001		
	Total BTEX	**0.005**		
PAHs	Naphtalene	27.12	Crysene	16.00
	Acenaphtylene	3.56	Benzo(a)anthracene	98.20
	Acenaphtene	91.22	Benzo(b)fluoranthene	102.60
	Fluorene	98.06	Benzo(k)fluoranthene	31.00
	Phénanthrene	250.03	Benzo(a)pyrene	44.37
	Anthracene	44.67	Dibenzo(a,h)anthracene	11.20
	Fluoranthene	182.67	Benzo(g,h,i)perylene	32.30
	Pyrene	139.80	Indeno(1,2,3-cd)pyrene	27.20
	Total		**1200**	

The soil samples slated for treatment revealed a total concentration of approximately 1200 mg/kg of polycyclic aromatic hydrocarbons (PAHs). Notably, phenanthrene emerged as the predominant pollutant within the soil under consideration, being recognized as a model pollutant.

2.3. Experimental Procedure

In this research, the process of oxidation was implemented using hydrogen peroxide (H_2O_2) and the Fenton reagent. The Fenton reagent involves the combination of hydrogen peroxide with ferrous ions (Fe^{2+}) acting as a catalyst, where a 0.5 M solution of heptahydrated ferrous sulfate ($FeSO_4$) was employed.

For each treatment, a soil sample containing pollutants (30 g) was mixed with distilled water in a 3:10 solid-to-liquid ratio within a 250 mL Erlenmeyer flask. The amount of water added was carefully determined to achieve a final solution volume (including the volume of the added oxidant) of approximately 100 mL. The soil–water mixture underwent magnetic stirring (300 rpm) for several minutes to ensure the creation of a homogeneous soil suspension. Following this, the oxidant was added gradually, with meticulous attention to preventing an excessive temperature rise. In the Fenton process, the catalyst was introduced first, followed by the oxidant. The Fenton (Fe(II)/Fe(III) + H_2O_2) process with a neutral pH maintains solubility, and thus enhances the production of oxidative species and extends the applicability of Fenton oxidation to a wider pH range [23–25].

Guided by prior studies on Fenton oxidation of crude oil hydrocarbons [26], concentrations of hydrogen peroxide and ferrous sulfate were chosen, encompassing two different molar ratios of H_2O_2:Fe^{2+} (50:1, 50:2, 100:1 and 100:2). The precise amounts of oxidant and catalyst for each sample are detailed in Table 3. Duplicate oxidation experiments were conducted under room temperature conditions (20 °C).

Table 3. Experimental conditions.

Oxidant	Tests	H_2O_2:Fe^{2+} Molar Ratio	Oxidant Concentration/M H_2O_2:Fe^{2+}
H_2O_2	H_1	25:0	5
	H_2	50:0	
	H_3	100:0	
	H_4	200:0	
Fenton	F_1	50:1	5:0.5
	F_2	50:2	5:0.5
	F_3	100:1	5:0.5
	F_4	100:2	5:0.5

2.4. Kinetics of PAH degradation in soil

In delving into the intricate dynamics of PAH degradation, we scrutinize the oxidation capacity as it evolves. The equilibrium of the chemical reaction manifests after a specified duration of interaction between the oxidant and the pollutant. The rate constant is extracted through the application of the model formulated by La Gergen [27], a choice made for its simplicity and its proven efficacy in the oxidation of organic compounds. The first-order and the second-order nonlinear reaction kinetics models were used to study the kinetics of PAH degradation using H_2O_2 and the Fenton oxidation process. The individual expressions were presented in the form of the equations below:

$$\frac{dC_t}{dt} = -k_1 C_t \quad (1)$$

$$\frac{dC_t}{dt} = -k_2 (C_t)^2 \quad (2)$$

where k_1 and k_2 represent the first-order and second-order kinetic rate constants, respectively; t is the reaction time and C_t is the PAH concentration at time t. Integrating Equations (1) and (2), give the following Equations (3) and (4):

$$C_t = C_0 e^{-k_1 t} \tag{3}$$

$$\frac{1}{C_t} = \frac{1}{C_0} + k_2 t \tag{4}$$

where k_1 and k_2 represent the rate constants of first-order and second-order kinetics model. C_0 and C_t are the initial concentration and the concentration at time t respectively.

To accurately ascertain the rate constant for the direct oxidation reaction initiated by the Fenton reagent, it is crucial to study it independently from the secondary reaction in which hydrogen peroxide (H_2O_2) with Fe^{2+} decomposes, generating $OH^{\bullet}$ radicals. In practical terms, this oxidation yields $OH^{\bullet}$ radicals that directly degrade the pollutant. The relationship between reaction time and the logarithmic concentration of various systems with different initial concentrations was determined under pH 8 conditions, with a reaction time of 60 min. A widely embraced model relies on reaction assumptions (Langmuir–Hinshelwood, 1921). The oxidation reaction catalyzed by H_2O_2 with Fe^{2+} is presumed to exhibit complete degradation capacity associated with a limited number of pollutant sites (monolayer coverage).

The reaction rate of H_2O_2 for a mass m of Fe^{2+} catalyst:

$$r = \frac{r_m}{m} = k[H_2O_2] \tag{5}$$

The degradation efficiency of the 16 PAHs was computed as follows:

$$E = \frac{\sum [PAH]_{initial} - \sum [PAH]_{final}}{\sum [PAH]_{initial}} \times 100 \tag{6}$$

where $\sum$[PAH] $_{initial}$ and $\sum$[PAH] $_{final}$ represent the concentrations of the 16 PAHs in the soil sample before and after oxidation (g/kg), respectively.

2.5. Gaussian Process Regression

Gaussian regression, also known as Gaussian process regression, stands as a sophisticated approach in machine learning for modeling probabilistic functions from observed data [28]. Unlike parametric regression models that impose specific assumptions on the data distribution, Gaussian processes embrace a non-parametric approach, thereby offering increased flexibility to represent complex relationships among variables [29]. In the realm of artificial intelligence, this model finds a plethora of applications, including time series prediction, modeling of unknown functions, and Bayesian optimization [30]. Fundamentally, a Gaussian process is defined by a probability distribution over functions, where each potential function is characterized by a mean and associated covariance [31]. The procedure for estimating the target function involves leveraging the properties of this distribution by using the observed data to update estimates of the mean and covariance [32]. This Bayesian approach offers the advantage of robust modeling while allowing precise quantification of uncertainty, which proves particularly useful in cases where data are limited or noisy [28]. Gaussian regression represents a powerful and flexible tool in the field of artificial intelligence, offering an elegant probabilistic method for modeling and predicting complex phenomena [30]. Its judicious use helps solve a variety of problems, thereby contributing to the advancement of research and applications in this ever-evolving domain [8].

In this comprehensive study, Gaussian process regression (GPR) served as the cornerstone for constructing a robust mathematical model aimed at predicting the reduced concentration (C/C_0), a critical parameter influenced by time (X1), H_2O_2 dose (X2), and Fe^{2+} dose (X3), all of which were carefully optimized within the scope of this research endeavor. With the dataset meticulously collected, a strategic division ensued, allocating 70% for training, and 30% for validation, ensuring the integrity and reliability of the model. To harness the full potential of GPR, a thorough exploration was conducted, scrutinizing 10 distinctive kernel functions, ranging from the conventional exponential and exponential squared to the more intricate Matern32, Matern52, quadratic rational, ARD exponential, ARD exponential squared, ARD Matern32, ARD Matern52, and ARD quadratic rational. This exploration extended further, delving into a myriad of basis functions, including constant, linear, Pure Quadratic, and zero, while meticulously fine-tuning the parameters—Kernel Scale [sigmaM, sigmaF], and sigma—of each kernel function to achieve optimal performance. Amidst this intricate optimization process, the assessment of the model's efficacy hinged upon two pivotal criteria: the coefficient of correlation, a measure of the model's ability to capture underlying trends, and the root mean square error (RMSE), a quantification of the model's predictive accuracy [29,33,34].

$$R = \frac{\sum_{i=1}^{N}\left(y_{\exp} - \overline{y}_{\exp}\right)\left(y_{pred} - \overline{y}_{pred}\right)}{\sqrt{\sum_{i=1}^{N}\left(y_{\exp} - \overline{y}_{\exp}\right)^2 \sum_{i=1}^{N}\left(y_{pred} - \overline{y}_{pred}\right)^2}} \quad (7)$$

$$\mathrm{RMSE} = \sqrt{\left(\frac{1}{\mathrm{N}}\right)\left(\sum_{\mathrm{i}=1}^{\mathrm{N}\Sigma}\left[\left(\mathrm{ypred}_{\exp}()\right)[]^2\right]()\right)} \quad (8)$$

where N is the number of data samples, K is the number of variables (inputs), y_{exp} and y_{pred} are the experimental and the predicted values respectively, $\overline{y}_{exp}$ and $\overline{y}_{pred}$ are respectively the average values of the experimental and the predicted values.

3. Results and Discussion

3.1. Effect of Oxidant Concentration

3.1.1. Effect of H_2O_2 Concentration

Figure 1 shows the kinetics of the variation in the C/C_0 ratio of PAHs as a function of H_2O_2 concentration for a duration of 60 min. The first series of experiments was carried out to investigate the effect of initial H_2O_2 concentration on HAP degradation kinetics. The C/C_0 ratios of PAHs decomposition as a function of time are shown in Figure 1. During treatment, the C/C_0 ratio decreases progressively from 1 to 0.429, 0.373, 0.303 and 0.244 for samples H_1, H_2, H_3, and H_4 respectively. However, Increasing H_2O_2 concentration above 25 mmol/samples results in a slight increase in the rate constant 0.013 min^{-1} 0.017 min^{-1} 0.019 min^{-1} and 0.023 min^{-1} for the first order and 0.017, 0.025, 0.03 and 0.035 L mol^{-1} min^{-1} for the second order for samples H_1, H_2, H_3 and H_4, respectively. This increase has been reported in several works including Aleboyeh, A et al. [35] and Chang, M. W. et al. [13]. where they attribute this to the fact that increasing the concentration of H_2O_2 above the optimum results in the transformation of the hydroxyl radicals to hydroperoxyl radicals, which are characterized by their lower oxidation capacity.

3.1.2. Effect of the Fenton Molar Ratio

Figure 2 depicts the kinetics portraying the fluctuation in the C/C_0 ratio of PAHs over a 60 min duration influenced by the Fenton molar ratio. This experimental series was designed to scrutinize the impact of varying the H_2O_2/Fe^{2+} molar ratio on the efficiency of PAH decomposition, as depicted in Figure 2. The variation in the H_2O_2/Fe^{2+} ratio leads to a decrease in the concentration ratio, reaching as low as 0.0017 for sample F4. The decrease

in the rate constant observed in Table 4 may be attributed to the augmented Fenton ion concentration, resulting in a diminished number of catalytically reactive sites.

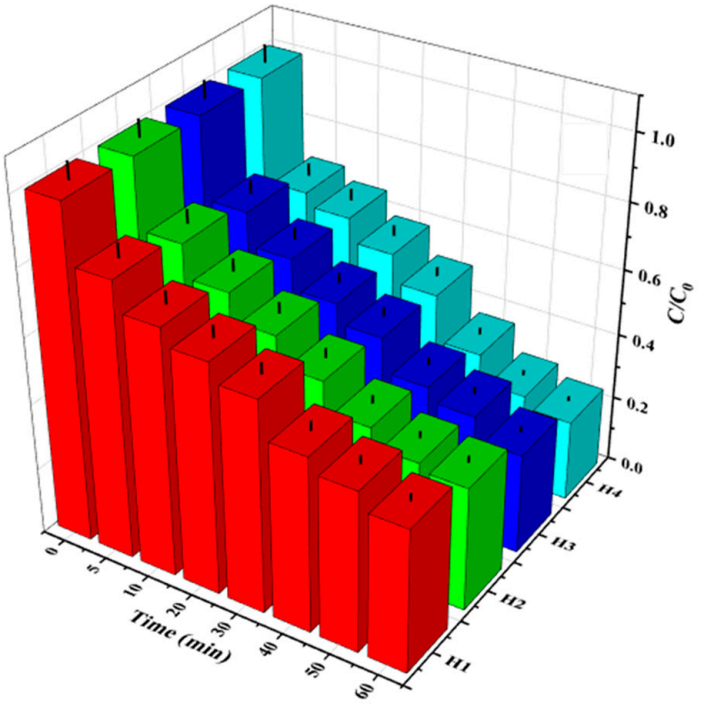

Figure 1. The variation of concentration ratios according to the dose of the oxidant H_2O_2 and time.

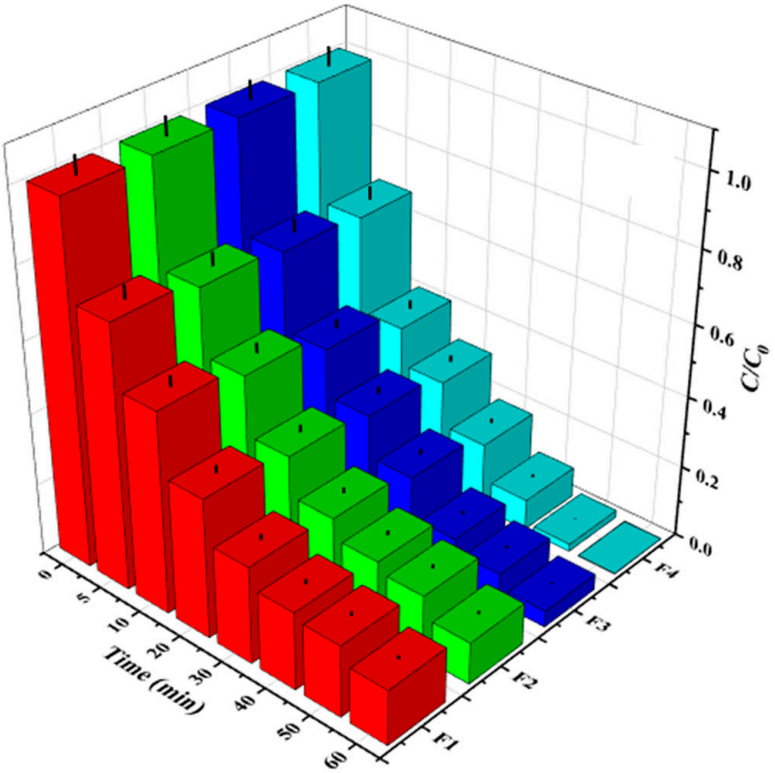

Figure 2. The variation of ratios according to the dose of the oxidant Fenton and time.

Table 4. Kinetics of the Oxidation Reaction in the Reaction Mixture.

1st Order			2nd Order		1st Order			2nd Order	
	R^2	$k \cdot min^{-1}$	R^2	$k \cdot L/mol \cdot min$		R^2	$k \cdot min^{-1}$	R^2	$k \cdot L/mol \cdot min$
H_1	0.95	0.013	0.97	0.017	F_1	0.97	0.039	0.997	0.069
H_2	0.95	0.017	0.98	0.025	F_2	0.97	0.043	0.997	0.077
H_3	0.94	0.019	0.97	0.03	F_3	0.98	0.055	0.975	0.097
H_4	0.94	0.023	0.95	0.035	F_4	0.98	0.066	0.958	0.118

3.2. Comparative Evaluation of Degradation Results Using H_2O_2 and H_2O_2/Fe^{2+}

PAH degradation efficiency ranged from 57%, 62.7%, 69.7%, and 75.6% for H_2O_2 assays H_1, H_2, H_3, and H_4, respectively. In the case involving the Fenton reagent, decomposition yields ranged from 84.7%, 88.3%, 95.5% and 99.9% for samples F_1, F_2, F_3, and F_4, respectively after 60 min of treatment (Figure 3). Pollutant destruction when using Fenton exceeded that of H_2O_2 alone, probably due to the fact that decomposition in the case of H_2O_2 is ensured by the highly reactive radicals formed, which are characterized by a short half-life, underlining the effectiveness of this oxidant for old contamination. During the Fenton process, the reaction between H_2O_2 and Fe^{2+} results in the production of mainly hydroxyl radicals, hydroperoxyl radicals and high-valent iron complexes, which can oxidize PAHs. Consequently, Fenton has been shown to be a potentially viable approach for the remediation of contaminated soils [5,24,36].

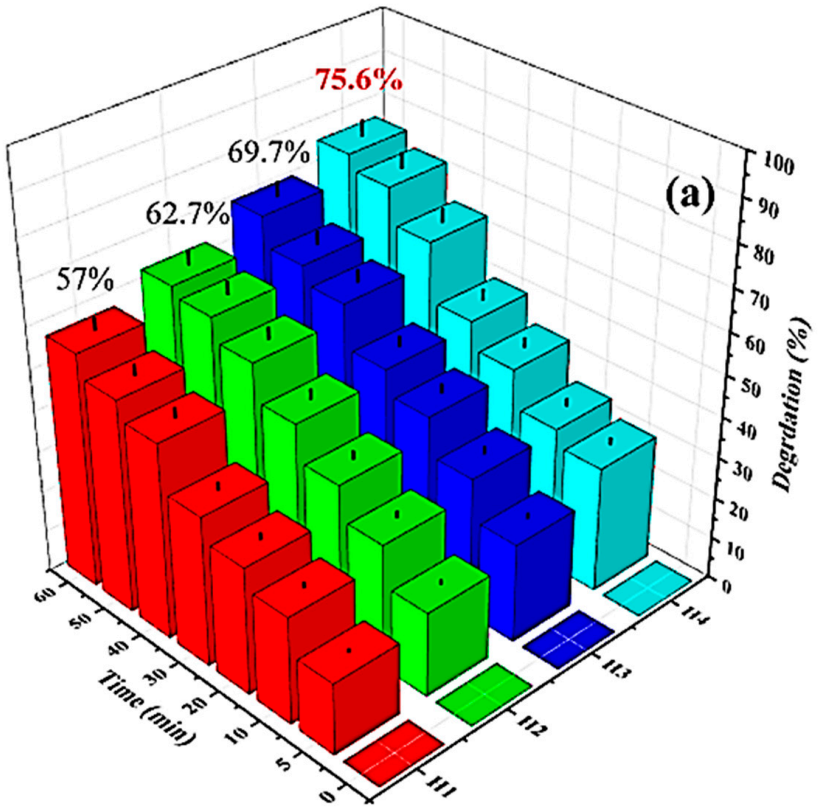

Figure 3. *Cont.*

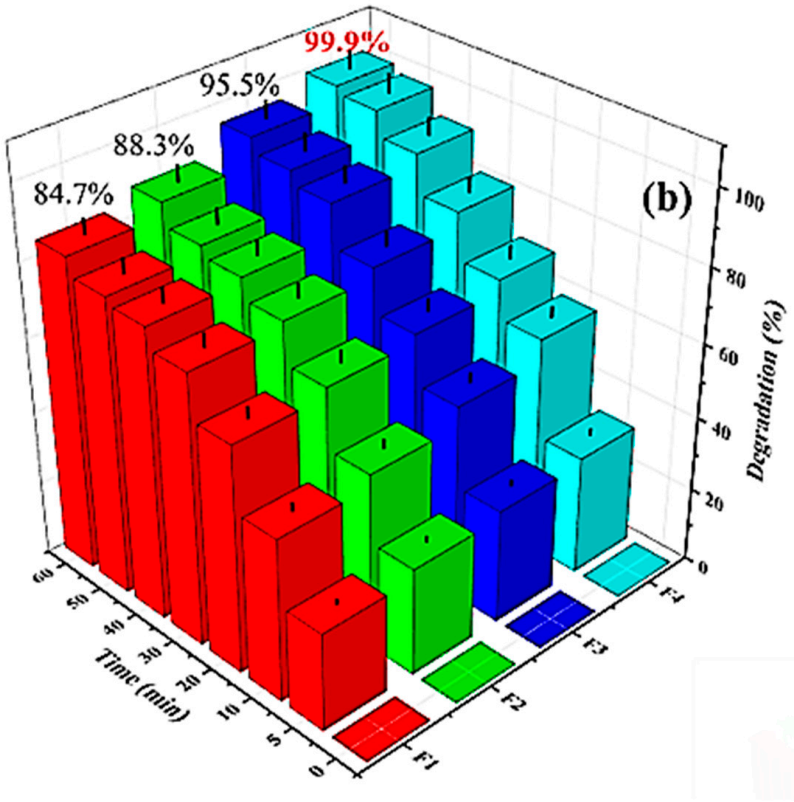

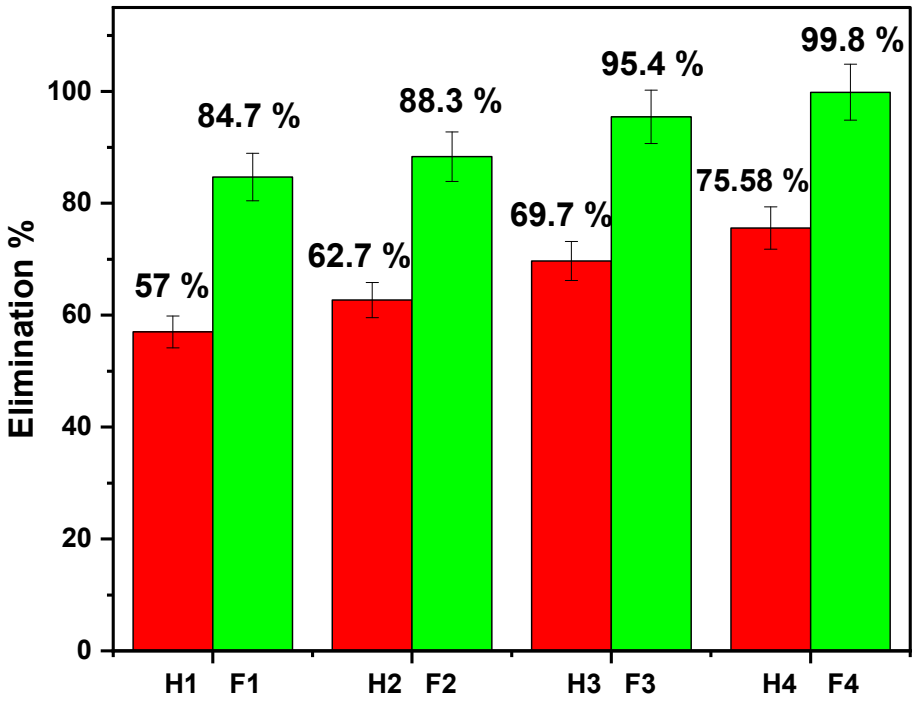

(**c**)

Figure 3. PAHs degradation rate (**a**) with H_2O_2 (**b**) with H_2O_2/Fe^{2+} (**c**) Comparative analysis of degradation rate using H_2O_2 and Fenton reagent.

3.3. pH Evolution during the Oxidation Process

The pH of the reaction system played a pivotal role in the degradation of polycyclic aromatic hydrocarbons (PAHs). The study of the initial pH effects was conducted for the reaction mixture using hydrogen peroxide, ranging between 7.1 and 8.01, as depicted in Figure 4a. As in the case of Fenton reagent utilization, a notable increase in pH from 7.3 to 8.6 was observed (Figure 4b), indicating the alkaline nature of the reaction mixture due to the production of hydroxyl ions (OH^-). This suggests that an elevation in the system's pH resulted in a substantial reduction in the elimination rate of PAHs [37–41]. Since PAHs are a series of non-ionizable organic compounds, this pH-dependent degradation behavior could be attributed to the characteristics of the oxidant. Therefore, the pH of the reaction system emerged as a critical factor in PAH degradation, exhibiting different first-order reaction rates in both cases and leading to an enhanced elimination of PAHs. To ensure the efficient presence of catalysis at neutral pH despite the low solubility of Fe(III), iron minerals naturally occurring in soils (normally iron in its oxidized state Fe(III)) have also been used as catalysts instead of soluble iron (Fe(II)) [42]. The progressive solubilization of the native iron minerals allows the decomposition of H_2O_2 and pollutants oxidation in soils without pH adjustment [43,44]. Similarly, heterogeneous Fenton reactions can effectively degrade refractory organic pollutants in soils at even circumneutral pH ranges [45].

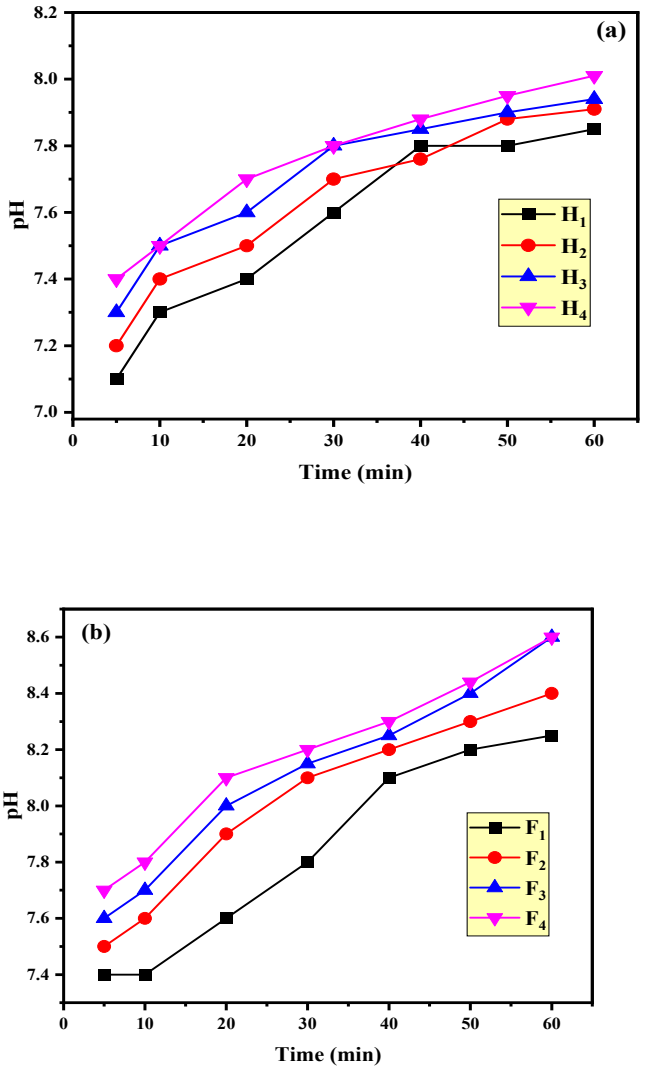

Figure 4. Variation of pH during chemical oxidation by H_2O_2 (**a**) and Fenton reagent (**b**).

3.4. Impact of Fenton Oxidation on Treated Soil

The infrared spectra of samples were acquired at room temperature employing a Perkin Elmer Fourier-transform infrared (FTIR) spectrometer. This instrument operates within the spectral range of 4000 to 400 cm^{-1}, encompassing both the mid-infrared and near-infrared regions, allowing for comprehensive analysis of molecular vibrations. Utilizing the attenuated total reflection (ATR) technique, the samples were prepared and measured. The ATR technique facilitates direct analysis of solid, liquid, and even thin film samples without the need for extensive sample preparation. Spectra were collected with a high spectral resolution of 4 cm^{-1}, ensuring fine detail and accuracy in the recorded vibrational spectra, thus enabling precise characterization of the chemical bonds present within the samples. The IR spectrum providing insight into the characteristic functional groups within soil contaminated by PAHs sheds light on the presence of alkyl groups (-CH_2-, =CH_2, CH_3) stemming from aliphatic chains (stretching vibrations) [46]. This is evident in the highly intense bands observed within the region of 2855.14 to 2921.14 cm^{-1} (represented in the Figure 5 by the grey color). Additionally, aromatic (C=C) groups exhibit peaks at 1420.66 cm^{-1} [47], (see the purple color in Figure 5a,b), and the existence of monosubstituted alkenes is indicated at 1009.33 cm^{-1} (represented by a cyan color). Furthermore, the functional group characteristic of a meta-disubstituted benzene compound is identified within the range of 691.26 to 797.5 cm^{-1} (represented by a green color) [48]. Upon closer examination of the peaks at varying concentrations of utilized Fenton, it becomes apparent that the alkyl group band at 2921.14 cm^{-1} is absent, along with the disappearance of peaks at 1420.66 cm^{-1}, confirming the nonexistence of aromatic groups [49]. Additionally, the peaks displayed from 1083.90 to 1085.58 cm^{-1} suggest lingering traces of alkenes in the treated samples. Notably, the functional group of a meta-disubstituted benzene compound persists at 798.93 cm^{-1}. These findings are visually represented in Figure 4a [50]. In the IR analysis of polluted soil treated with hydrogen peroxide as the oxidant, as presented in Figure 4b, a resemblance to the Fenton-treated samples is observed, with the absence of the alkyl group band at 2921.14 cm^{-1} and the disappearance of peaks at 1420.66 cm^{-1}, indicating the nonexistence of aromatic groups. Traces of alkenes are still discernible in the peaks ranging from 1083.75 to 1087.22 cm^{-1}. The functional group of a meta-disubstituted benzene compound is also evident at 798.93 cm^{-1} in the treated samples. These results elucidate the significant elimination rate, attributed to the comprehensive oxidation of PAHs and the efficacy of the chosen oxidant.

Comparing the IR spectra of polluted soil to soil treated with both oxidants underscores the equal efficiency in achieving complete hydrocarbon degradation. Peak intensity observations reveal that F is lower than PS, while in H, it surpasses PS (indicating the presence of organic OH groups). Although a small amount of [H_2O_2] for F_1 and F_2 suffices, a larger quantity is required for H_3 and H_4 to decrease peak intensity.

The suggestion to employ a concentrated hydrogen peroxide solution for treating polycyclic aromatic hydrocarbons (PAHs) attached to non-aqueous phase liquids is rooted in the development of an alternative reductive pathway. This pathway demonstrates efficacy in breaking down organic compounds that exhibit resistance to hydroxyl radicals. Under robust Fenton conditions, the overall mechanism proposes the interaction of adsorbed PAHs with either aqueously present or surface-generated hydroxyl radicals ($OH^{\bullet}$).

This proposed mechanism underscores the intricate interplay of hydrogen peroxide and iron ions, leading to the generation of hydroxyl radicals ($OH^{\bullet}$). The ensuing oxidative power of these radicals facilitates the degradation of PAHs adsorbed onto non-aqueous phase liquids.

This interpretation aligns with the experimental results, emphasizing the significance of understanding the underlying chemical processes for optimizing the degradation efficiency of persistent organic pollutants in contaminated soil.

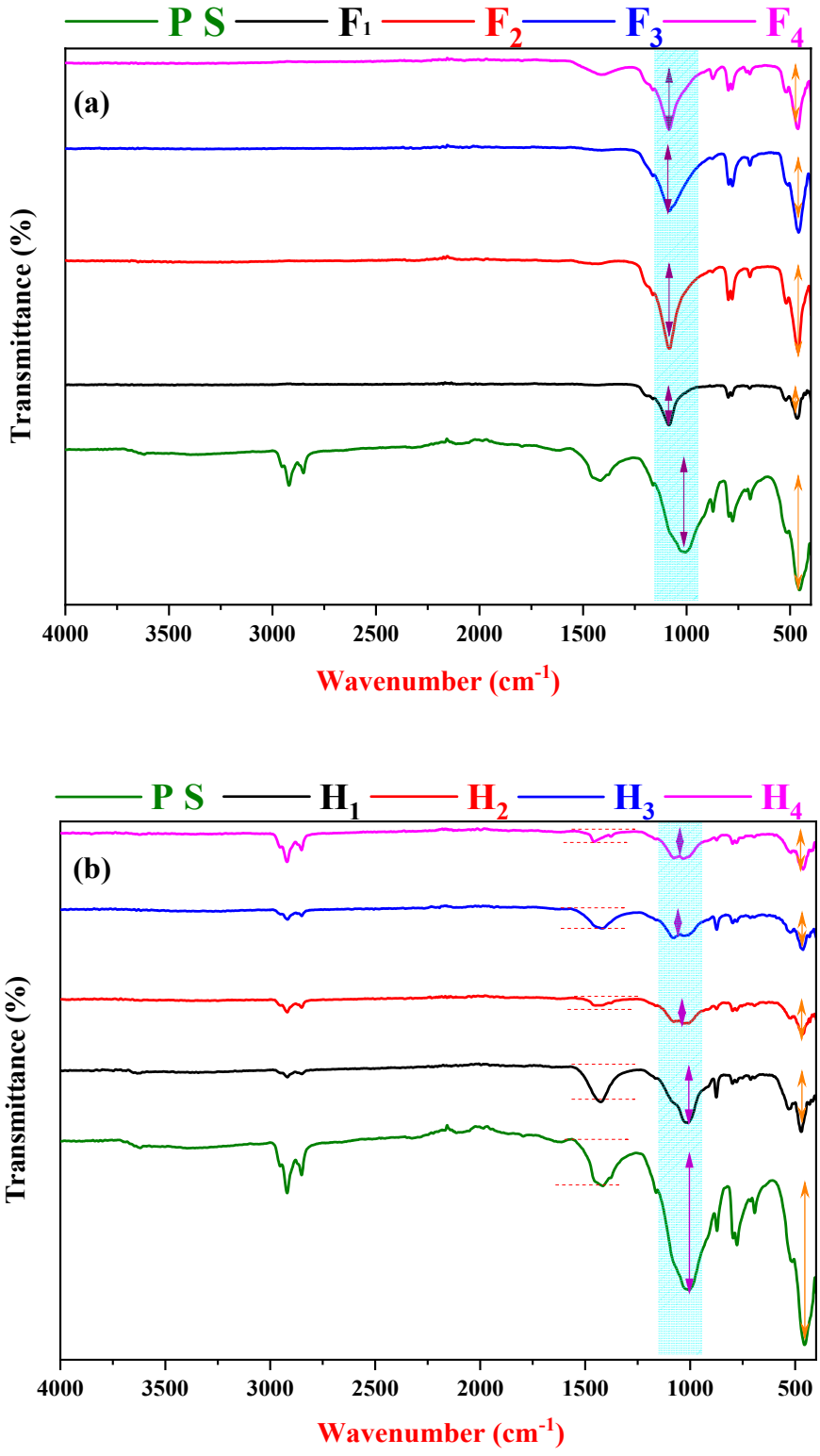

Figure 5. (**a**) FTIR spectrum of polluted soil before and after treatment by the Fenton process (**b**) FTIR spectrum of polluted soil before and after treatment by hydrogen peroxide.

3.5. Proposed Mechanism of the Hydrogen Peroxide and Fenton Degradation

The mechanisms of polycyclic aromatic hydrocarbons (PAHs) degradation by hydrogen peroxide (H_2O_2) alone and the Fenton process (H_2O_2/Fe^{2+}) share a common basis of highly reactive hydroxyl radicals ($OH^{\bullet}$) formation [51], as shown in Figure 6. When H_2O_2 is used alone, it spontaneously decomposes to generate $OH^{\bullet}$, which attacks PAHs, breaking

them down into smaller fragments. In the Fenton process, the addition of iron (II) (Fe^{2+}) acts as a catalyst, promoting more efficient $OH^{\bullet}$ formation. Fe^{2+} reduces H_2O_2, generating $OH^{\bullet}$ and regenerating Fe^{2+} in the process. The $OH^{\bullet}$ then attack PAHs [52], leading to their degradation. Both mechanisms involve PAH decomposition by hydroxyl radicals, but the Fenton process, with the addition of Fe^{2+}, exhibits greater efficiency in generating more $OH^{\bullet}$ to accelerate the degradation process [53].

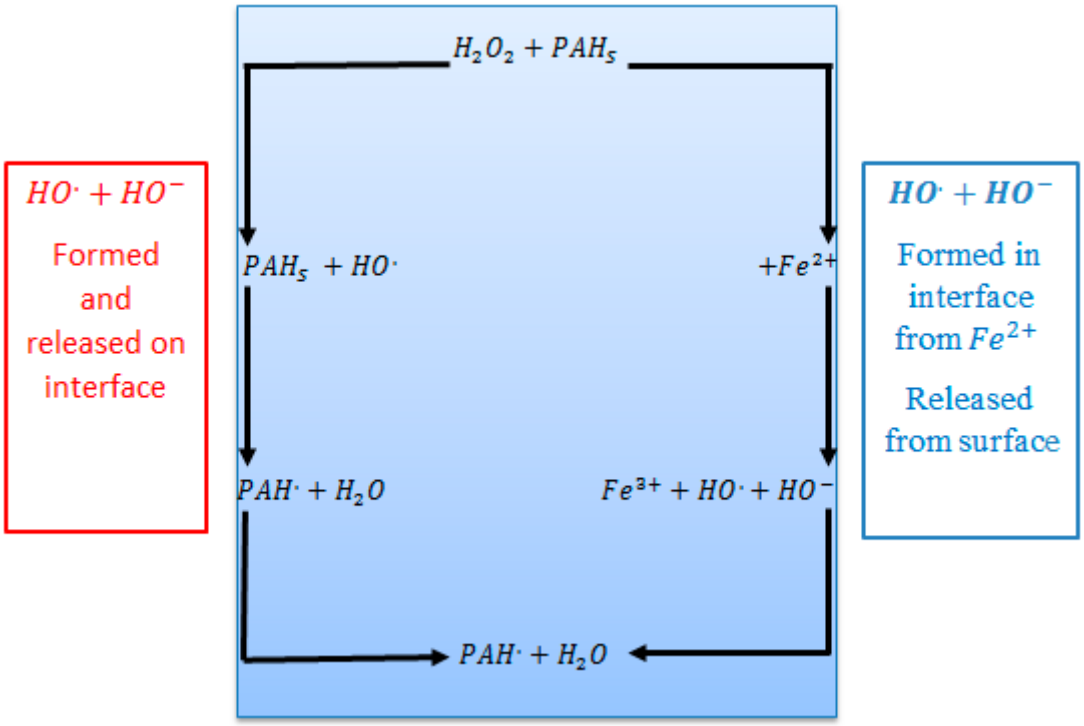

Figure 6. Mechanism of PAH degradation using H_2O_2 and H_2O_2/Fe^{2+}.

Reactions for the H_2O_2 Mechanism:
Decomposition of hydrogen peroxide:

$$H_2O_2 \rightarrow OH^- + OH^{\bullet} \quad (9)$$

Attack of hydroxyl radicals ($OH^{\bullet}$) on PAHs:

$$HAP + OH^{\bullet} \rightarrow HAP^{\bullet} + H_2O \quad (10)$$

Reactions for the Fenton Process (H_2O_2/Fe^{2+}):
Formation of hydroxyl radicals ($OH^{\bullet}$):

$$Fe^{2+} + H_2O_2 \rightarrow Fe^{3+} + OH^- + OH^{\bullet} \quad (11)$$

Attack of hydroxyl radicals on PAHs:

$$HAP + OH^{\bullet} \rightarrow HAP^{\bullet} + H_2O \quad (12)$$

Chain reactions:
Resulting fragments from PAHs can themselves react with hydroxyl radicals, thus initiating a chain reaction.
Formation of oxidized species:
Resulting degradation products may undergo further oxidation reactions, forming oxidized compounds that are easier to degrade or eliminate.

Regeneration of iron (II) (Fe^{2+}):

$$Fe^{3+} + e^{-} \rightarrow Fe^{2+} \quad (13)$$

The iron (III) (Fe^{3+}) formed during the reaction is reduced back to iron (II) (Fe^{2+}) by electrons released in the reaction, allowing for the regeneration of the ferrous catalyst.

3.6. Gaussian Process Regression

As previously indicated, to obtain the best model, we explored a diverse range of kernel functions, from conventional ones such as exponential and exponential squared, to more intricate ones such as Matern32, Matern52, quadratic rational, ARD exponential, ARD exponential squared, ARD Matern32, ARD Matern52, and ARD quadratic rational. This exploration further extended to encompass a myriad of basis functions, including constant, linear, PureQuadratic, and zero. Simultaneously, the parameters—Kernel Scale [sigmaM, sigmaF], and sigma—of each kernel function were meticulously fine-tuned to achieve optimal performance. The results of the best model obtained were represented in Table 5, highlighting the values of Kernel Scale [sigmaM, sigmaF], and sigma, the number of parameters, as well as the correlation coefficients and RMSE for each phase of the study. This reminder helps to contextualize the forthcoming results within the utilized methodology and will facilitate their interpretation.

Table 5. Performances of the GPR model.

Kernel Function	Basis Function	Kernel Scale		Sigma	Quantite	R			RMSE (1.0 e-03)		
		SigmaM	SigmaF			Train	Val	All	Train	Val	All
ARD-Exponential	Constant	18.8299 160.0958 51.8017	0.6258	0.0029	44	1.0000	0.9997	0.9999	0.1392	0.0212	0.1173

The results from the Table 5 demonstrate exceptional performance of the model at each phase of optimization. The use of the ARD-Exponential kernel function combined with a constant basis function appears to be the optimal configuration for achieving these high performances. This combination allows for flexible adaptation to the data while ensuring precise modeling of relationships between input variables. Additionally, the coefficient of correlation (R) reaching the maximum value of 1 for all phases indicates a perfect correlation between predicted and actual values during training, validation, and across all data. This underscores the model's ability to effectively capture trends and relationships between variables. Similarly, the extremely low values of RMSE (root mean square error) for each phase, notably 0.1392×10^{-3} for training, 0.0212×10^{-3} for validation, and 0.1173×10^{-3} for all data, denote remarkable precision in the model's predictions, with minimal deviations between predicted and actual values. Regarding the choices of kernel and basis functions, these results confirm the reliability and effectiveness of the optimized model in predicting reduced concentration, highlighting its potential application across various research and industry domains.

These results are visually presented in Figure 7, providing a graphical representation of the findings.

3.6.1. Residual Analysis of Model GPR

A detailed residual analysis was carried out to provide a comprehensive validation of the model's efficacy and reliability. Initially, the experimental and predicted values were overlaid on a graph (Figure 8a), enabling a visual comparison to assess their alignment. This graphical representation facilitated the identification of any systematic deviations or patterns in the model's predictions across different phases [33]. Additionally, a second

analytical approach was employed, where an error histogram was constructed to visualize the distribution of residuals for each phase (Figure 8b) [28,33]. This method allowed for a deeper exploration of the discrepancies between predicted and observed values, shedding light on potential outliers or areas of inconsistency. By combining these techniques, a thorough examination of the model's performance was achieved, offering valuable insights into its predictive capabilities and highlighting any areas for refinement or further investigation.

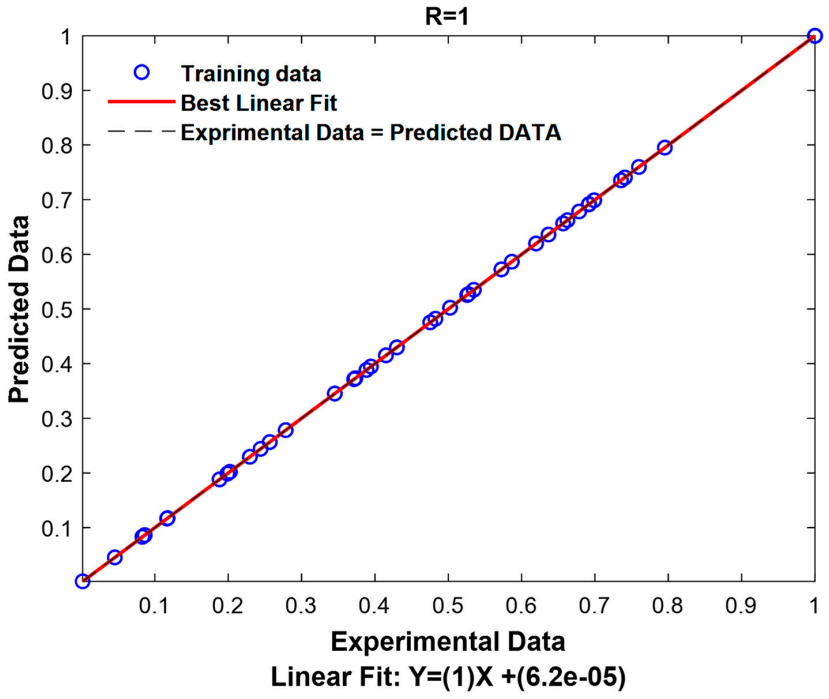

(**a**)

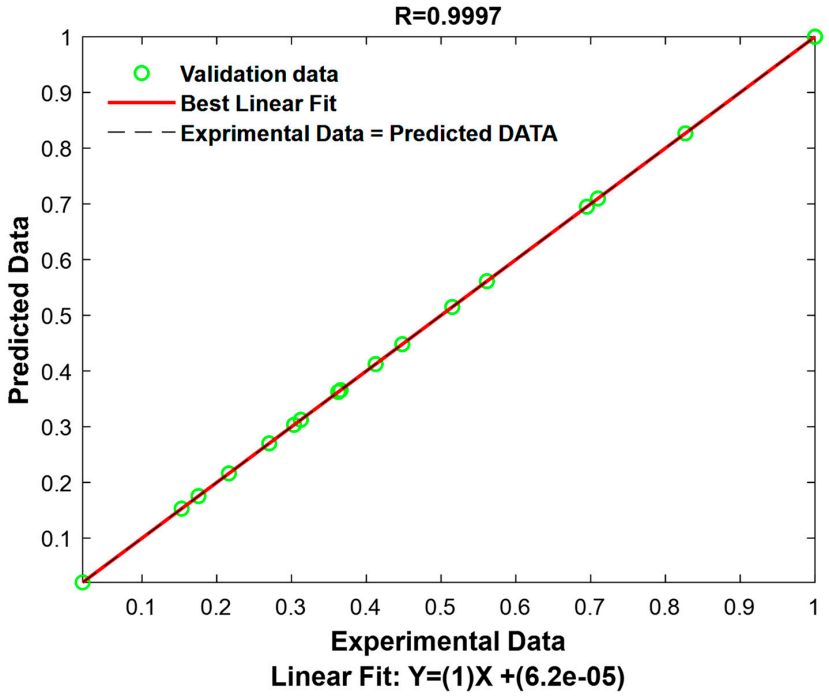

(**b**)

Figure 7. *Cont*.

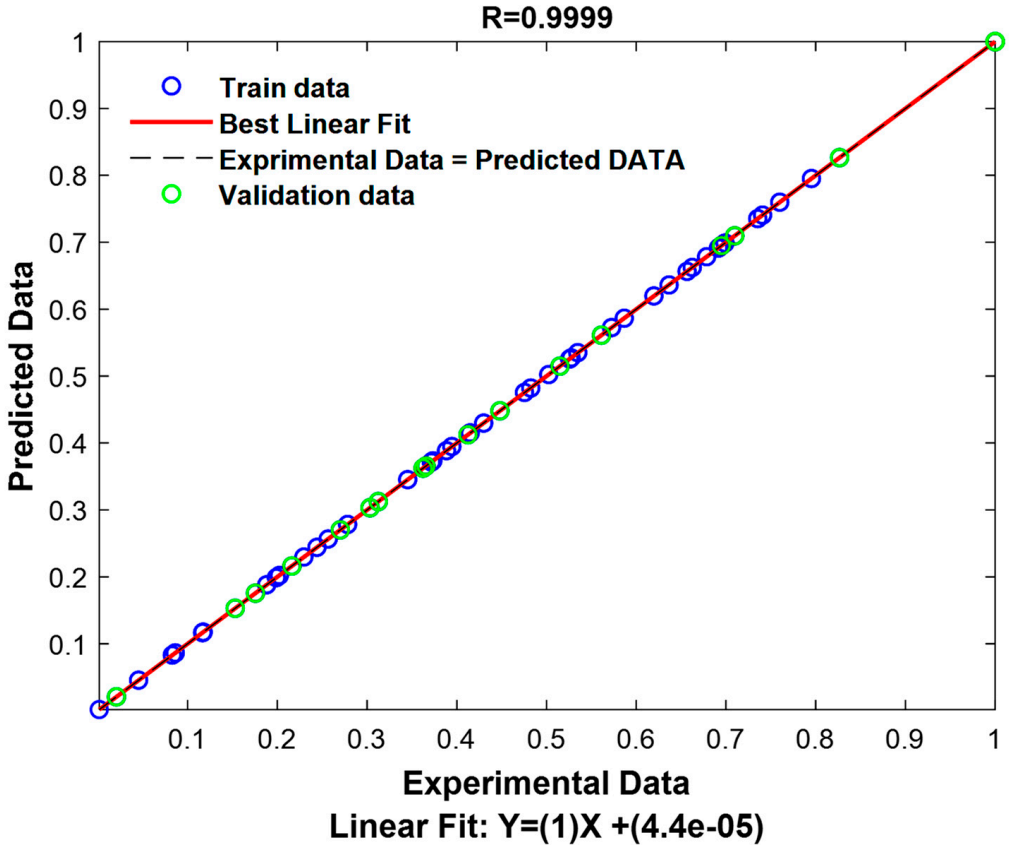

Figure 7. Relationship between the experimental and the GPR model predicted values: (**a**) Training phase, (**b**) validation phase, and (**c**) all phase.

The findings underscore a compelling coherence between the experimental data and the model's predictions (Figure 8a), affirming the robustness of the developed model. This harmonious alignment not only validates the model's capacity to faithfully capture the intricate nuances within the dataset but also attests to its reliability in providing accurate predictions. Moreover, this alignment was further accentuated by a meticulous error analysis, meticulously illustrated through a histogram depiction (Figure 8b). Noteworthy is the discernible clustering of errors within a remarkably narrow range, confined within the interval of [−0.0003, 0.0003] (Figure 8b). This nuanced examination reveals a striking precision in the model's predictions, with the overwhelming majority of discrepancies being minute. Such precision reinforces the model's resilience and aptitude, bolstering its applicability across various domains.

3.6.2. Optimization and Validation of the Optimum Conditions

The Improved Grey Wolf Optimizer algorithm (IGWO) emerged as a cornerstone in achieving optimization [33,34]. Leveraging its robust optimization capabilities, the algorithm facilitated the attainment of an optimal solution (minimization of C/C_0), which was subsequently rigorously validated within the laboratory setting. Following this validation, a thorough examination of predictive accuracy ensued, entailing the meticulous calculation of errors between predicted and experimental values. These insightful results were meticulously compiled and presented in Table 6, offering a detailed portrayal of the model's predictive performance and its alignment with experimental data.

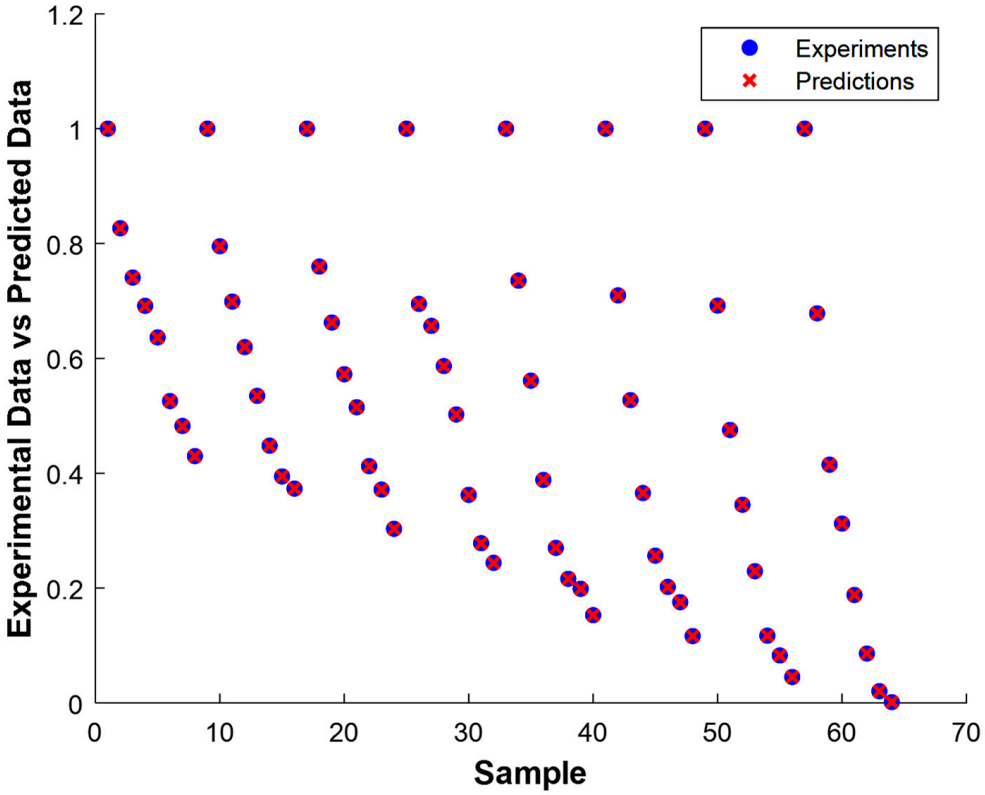

(**a**)

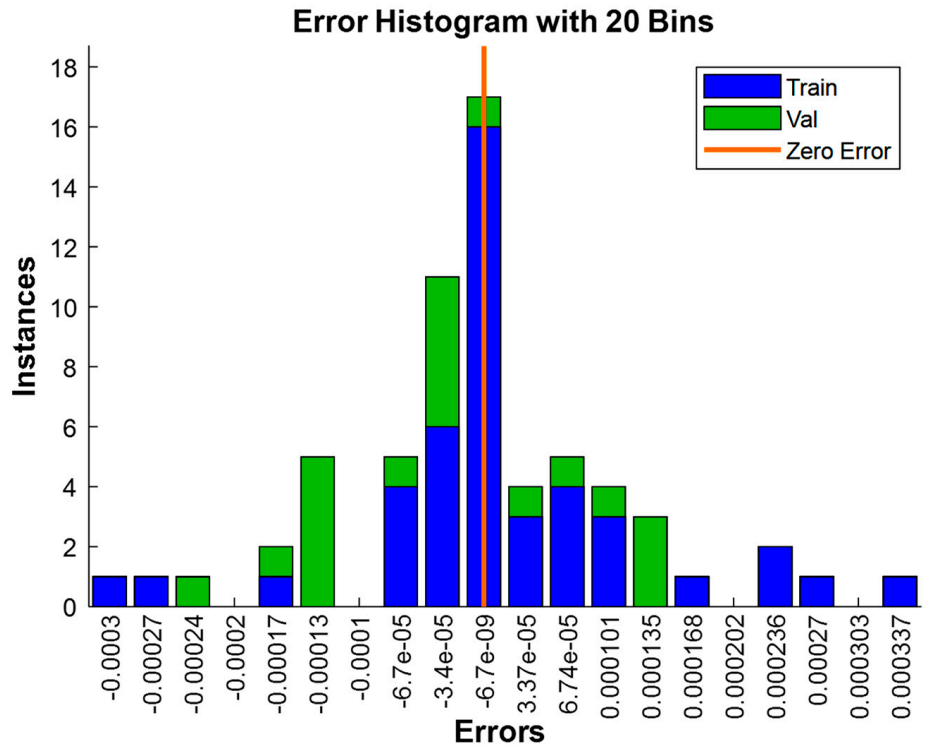

(**b**)

Figure 8. Residuals relating to the model established: (**a**) Relationship between experimental data and the predicted data of samples, and (**b**) Instances distribution of errors.

Table 6. Comparison between actual and predicted responses at optimum conditions.

X_1 = 60. X_2 = 200. and X_3 = 2	
C/C_0 experimental values	0.001
C/C_0 predicted values	0
Error	0.001

Where:

$$Error = Experimental\ response - Predicted\ response \quad (14)$$

The results presented in Table 6 demonstrate a remarkable consistency between the experimental values of C/C_0 (reduced concentration) and the model predictions. Initially, the experimental measurements revealed a value of 0.001, while the model had anticipated a value of 0. Although this slight disparity results in a prediction error of 0.001, it nevertheless underscores the precision of the model in its forecasts. This observation sheds light on the undeniable effectiveness and reliability of the model in representing the studied phenomena.

3.6.3. Interface for Optimization and Prediction

To enhance the predictive capabilities of our research, we have developed a bespoke application using MATLAB (Figure 9). This application serves the purpose of optimizing the minimization of C/C_0, a critical parameter in our study, employing the IGWO algorithm. This optimization process is founded upon the robust model created through GPR, which accurately captures the underlying dynamics of the system under investigation. By integrating these advanced computational techniques, our methodology not only ensures the precision of our predictions but also provides a streamlined approach for further exploration and analysis in our research domain.

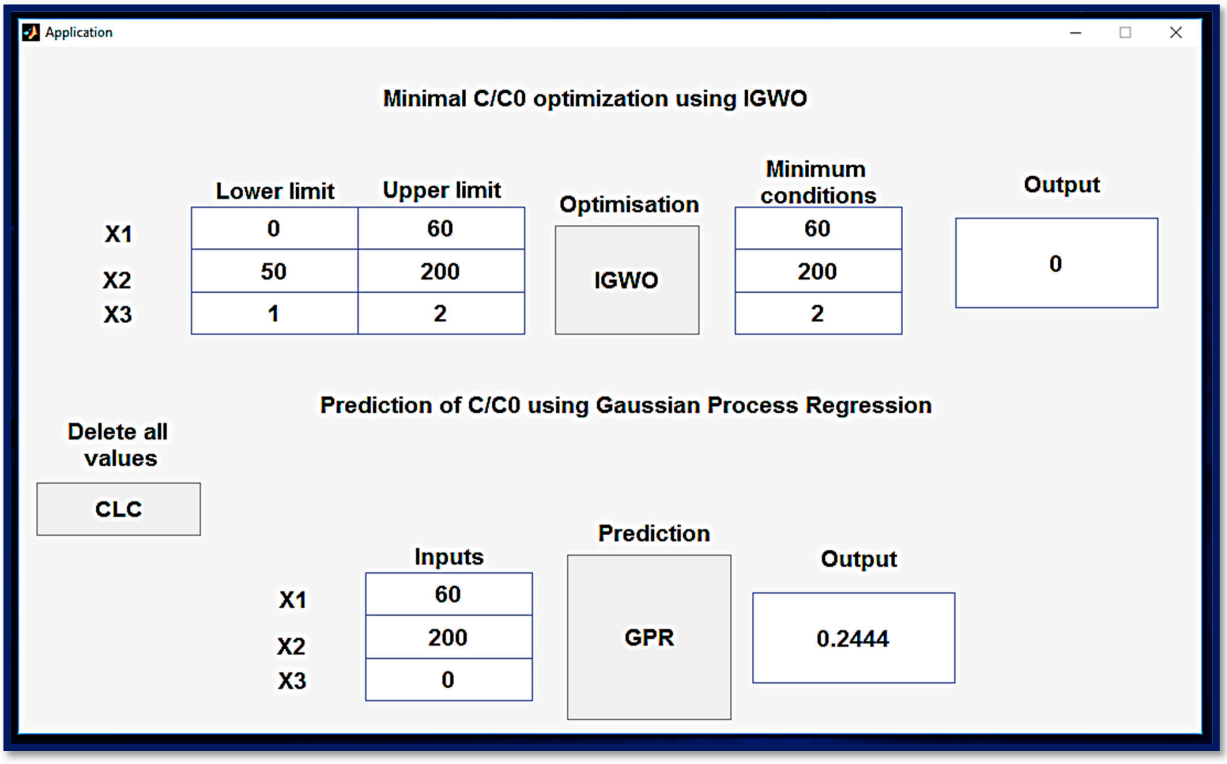

Figure 9. MATLAB interface for optimization and prediction of C/C0 using IGWO and GPR.

4. Conclusions

This study provides valuable insights into the breakdown kinetics of polycyclic aromatic hydrocarbons (PAHs) using both hydrogen peroxide (H_2O_2) and the Fenton process (H_2O_2/Fe^{2+}). The results demonstrate the effectiveness of both H_2O_2 and the Fenton process in degrading PAHs, with the latter showing greater efficiency, achieving decomposition rates ranging from 84.7% to 99.9%. The pH changes during oxidation significantly affect PAH degradation, underlining the importance of maintaining optimal pH levels for successful remediation. Additionally, Fourier-transform infrared (FTIR) spectroscopy analysis confirms significant PAH removal post-treatment, with both oxidants exhibiting similar efficacy in achieving complete hydrocarbon degradation. The mechanisms underlying PAH degradation, primarily through the formation of hydroxyl radicals, highlight the enhanced efficiency of the Fenton process facilitated by Fe^{2+} catalysis. The Gaussian process regression (GPR) model, especially using the ARD-Exponential kernel function, accurately predicts reduced concentrations, demonstrating superior performance. Utilizing the Improved Grey Wolf Optimizer algorithm allows for the optimization of reaction conditions, resulting in strong agreement between experimental and predicted values. Furthermore, the creation of a MATLAB interface offers a user-friendly platform for efficient optimization and prediction, catering to the needs of researchers and practitioners. In conclusion, this integrated approach presents promising avenues for enhancing oxidant-based PAH remediation techniques, particularly in soil remediation efforts. Future research endeavors should focus on refining optimization strategies and exploring additional factors influencing PAH degradation kinetics, ultimately advancing the effectiveness of remediation in real-world environmental contexts.

Author Contributions: Conceptualization, M.S., R.K., N.M.-M., K.M., D.M., S.L., O.B., H.T., J.Z. and A.A.; Methodology, M.S., R.K., N.M.-M., H.T., J.Z. and A.A.; Software, R.K., N.M.-M. and J.Z.; Validation, M.S., R.K., N.M.-M., K.M., D.M., O.B., H.T., J.Z. and A.A.; Formal analysis, M.S., R.K., N.M.-M., K.M., D.M., S.L., O.B., H.T., J.Z. and A.A.; Investigation, M.S., R.K., N.M.-M., K.M., D.M., S.L., O.B., H.T., J.Z. and A.A.; Resources, D.M., H.T., J.Z. and A.A.; Writing—original draft, M.S., R.K. and H.T.; Writing—review & editing, N.M.-M., K.M., D.M., S.L., O.B., J.Z. and A.A.; Visualization, M.S., R.K., N.M.-M., K.M., D.M., S.L., O.B., H.T., J.Z. and A.A.; Supervision, R.K., N.M.-M. and A.A.; Project administration, H.T., J.Z. and A.A. All authors have read and agreed to the published version of the manuscript.

Funding: This research received no external funding.

Data Availability Statement: Data are contained within the article.

Conflicts of Interest: The authors declare no conflict of interest.

References

1. Song, X.; Xu, Y.; Li, G.; Zhang, Y.; Huang, T.; Hu, Z. Isolation, Characterization of Rhodococcus Sp. P14 Capable of Degrading High-Molecular-Weight Polycyclic Aromatic Hydrocarbons and Aliphatic Hydrocarbons. *Mar. Pollut. Bull.* **2011**, *62*, 2122–2128. [CrossRef]
2. Gou, Y.; Zhao, Q.; Yang, S.; Wang, H.; Qiao, P.; Song, Y.; Cheng, Y.; Li, P. Removal of Polycyclic Aromatic Hydrocarbons (PAHs) and the Response of Indigenous Bacteria in Highly Contaminated Aged Soil after Persulfate Oxidation. *Ecotoxicol. Environ. Saf.* **2020**, *190*, 110092. [CrossRef]
3. Li, G.; Huang, S.; Zhu, N.; Yuan, H.; Ge, D. Near-Infrared Responsive Upconversion Glass-Ceramic@ BiOBr Heterojunction for Enhanced Photodegradation Performances of Norfloxacin. *J. Hazard. Mater.* **2021**, *403*, 123981. [CrossRef] [PubMed]
4. Madi, K.; Chebli, D.; Ait Youcef, H.; Tahraoui, H.; Bouguettoucha, A.; Kebir, M.; Zhang, J.; Amrane, A. Green Fabrication of ZnO Nanoparticles and ZnO/rGO Nanocomposites from Algerian Date Syrup Extract: Synthesis, Characterization, and Augmented Photocatalytic Efficiency in Methylene Blue Degradation. *Catalysts* **2024**, *14*, 62. [CrossRef]
5. Gou, Y.; Yang, S.; Cheng, Y.; Song, Y.; Qiao, P.; Li, P.; Ma, J. Enhanced Anoxic Biodegradation of Polycyclic Aromatic Hydrocarbons (PAHs) in Aged Soil Pretreated by Hydrogen Peroxide. *Chem. Eng. J.* **2019**, *356*, 524–533. [CrossRef]
6. Lemaire, J.; Mora, V.; Faure, P.; Hanna, K.; Buès, M.; Simonnot, M.-O. Chemical Oxidation Efficiency for Aged, PAH-Contaminated Sites: An Investigation of Limiting Factors. *J. Environ. Chem. Eng.* **2019**, *7*, 103061. [CrossRef]
7. Ma, F.; Zhang, Q.; Wu, B.; Peng, C.; Li, N.; Li, F.; Gu, Q. Treatment of PAH-Contaminated Soil Using Cement-Activated Persulfate. *Environ. Sci. Pollut. Res.* **2018**, *25*, 887–895. [CrossRef]

8. Tang, L.; Zhang, X.; Li, Z.; Gudda, F.O.; Waigi, M.G.; Wang, J.; Liu, H.; Gao, Y. Enhanced PAHs-Contaminated Site Soils Remediation by Mixed Persulfate and Calcium Peroxide. *J. Environ. Manag.* **2022**, *306*, 114363. [CrossRef]
9. Li, Y.; Liao, X.; Huling, S.G.; Xue, T.; Liu, Q.; Cao, H.; Lin, Q. The Combined Effects of Surfactant Solubilization and Chemical Oxidation on the Removal of Polycyclic Aromatic Hydrocarbon from Soil. *Sci. Total Environ.* **2019**, *647*, 1106–1112. [CrossRef] [PubMed]
10. Zhou, Z.; Liu, X.; Sun, K.; Lin, C.; Ma, J.; He, M.; Ouyang, W. Persulfate-Based Advanced Oxidation Processes (AOPs) for Organic-Contaminated Soil Remediation: A Review. *Chem. Eng. J.* **2019**, *372*, 836–851. [CrossRef]
11. Zhang, T.; Liu, Y.; Zhong, S.; Zhang, L. AOPs-Based Remediation of Petroleum Hydrocarbons-Contaminated Soils: Efficiency, Influencing Factors and Environmental Impacts. *Chemosphere* **2020**, *246*, 125726. [CrossRef]
12. Alekseevich, V.M.; Viktorovich, A.O.; Rinatovich, T.A.; Vladimirovich, B.A.; Failevich, M.I. Study of Chemical Additives for Optimization of Binary Systems Used for Downhole Thermochemical Treatment of Heavy Oil. *Processes* **2023**, *11*, 2465.
13. Cheng, M.; Zeng, G.; Huang, D.; Lai, C.; Xu, P.; Zhang, C.; Liu, Y.; Wan, J.; Gong, X.; Zhu, Y. Degradation of Atrazine by a Novel Fenton-like Process and Assessment the Influence on the Treated Soil. *J. Hazard. Mater.* **2016**, *312*, 184–191. [CrossRef]
14. Neyens, E.; Baeyens, J. A Review of Classic Fenton's Peroxidation as an Advanced Oxidation Technique. *J. Hazard. Mater.* **2003**, *98*, 33–50. [CrossRef]
15. Cheng, M.; Zeng, G.; Huang, D.; Lai, C.; Xu, P.; Zhang, C.; Liu, Y. Hydroxyl Radicals Based Advanced Oxidation Processes (AOPs) for Remediation of Soils Contaminated with Organic Compounds: A Review. *Chem. Eng. J.* **2016**, *284*, 582–598. [CrossRef]
16. Gan, S.; Yap, C.L.; Ng, H.K. Investigation of the Impacts of Ethyl Lactate Based Fenton Treatment on Soil Quality for Polycyclic Aromatic Hydrocarbons (PAHs)-Contaminated Soils. *J. Hazard. Mater.* **2013**, *262*, 691–700. [CrossRef] [PubMed]
17. Bellanger, B.; Huon, S.; Steinmann, P.; Chabaux, F.; Velasquez, F.; Valles, V.; Arn, K.; Clauer, N.; Mariotti, A. Oxic–Anoxic Conditions in the Water Column of a Tropical Freshwater Reservoir (Pena-Larga Dam, NW Venezuela). *Appl. Geochem.* **2004**, *19*, 1295–1314. [CrossRef]
18. Yang, K.; Nam, T.; Nam, K.; Kim, Y.-J. Characteristics of Heavy Metal Contamination by Anthropogenic Sources in Artificial Lakes of Urban Environment. *KSCE J. Civ. Eng.* **2016**, *20*, 121–128. [CrossRef]
19. Xu, Y.; Che, T.; Li, Y.; Fang, C.; Dai, Z.; Li, H.; Xu, L.; Hu, F. Remediation of Polycyclic Aromatic Hydrocarbons by Sulfate Radical Advanced Oxidation: Evaluation of Efficiency and Ecological Impact. *Ecotoxicol. Environ. Saf.* **2021**, *223*, 112594. [CrossRef] [PubMed]
20. Xia, C.; Liu, Q.; Zhao, L.; Wang, L.; Tang, J. Enhanced Degradation of Petroleum Hydrocarbons in Soil by FeS@ BC Activated Persulfate and Its Mechanism. *Sep. Purif. Technol.* **2022**, *282*, 120060. [CrossRef]
21. Ranc, B.; Faure, P.; Croze, V.; Simonnot, M. Selection of Oxidant Doses for in Situ Chemical Oxidation of Soils Contaminated by Polycyclic Aromatic Hydrocarbons (PAHs): A Review. *J. Hazard. Mater.* **2016**, *312*, 280–297. [CrossRef]
22. Ouriache, H.; Arrar, J.; Namane, A.; Bentahar, F. Treatment of Petroleum Hydrocarbons Contaminated Soil by Fenton like Oxidation. *Chemosphere* **2019**, *232*, 377–386. [CrossRef]
23. Zhang, Y.; Zhou, M. A Critical Review of the Application of Chelating Agents to Enable Fenton and Fenton-like Reactions at High pH Values. *J. Hazard. Mater.* **2019**, *362*, 436–450. [CrossRef] [PubMed]
24. Usman, M.; Hanna, K.; Haderlein, S. Fenton Oxidation to Remediate PAHs in Contaminated Soils: A Critical Review of Major Limitations and Counter-Strategies. *Sci. Total Environ.* **2016**, *569*, 179–190. [CrossRef]
25. Ahile, U.J.; Wuana, R.A.; Itodo, A.U.; Sha'Ato, R.; Dantas, R.F. A Review on the Use of Chelating Agents as an Alternative to Promote Photo-Fenton at Neutral pH: Current Trends, Knowledge Gap and Future Studies. *Sci. Total Environ.* **2020**, *710*, 134872. [CrossRef]
26. Satilmis, I.; Schrader, W. Studying the Fenton Treatment of Polycyclic Aromatic Compounds in a Highly Contaminated Soil with Different Modifiers by High Resolution Mass Spectrometry. *J. Hazard. Mater. Adv.* **2022**, *8*, 100200. [CrossRef]
27. Checa-Fernandez, A.; Santos, A.; Romero, A.; Dominguez, C.M. Application of Chelating Agents to Enhance Fenton Process in Soil Remediation: A Review. *Catalysts* **2021**, *11*, 722. [CrossRef]
28. Mechati, S.; Zamouche, M.; Tahraoui, H.; Filali, O.; Mazouz, S.; Bouledjemer, I.N.E.; Toumi, S.; Triki, Z.; Amrane, A.; Kebir, M. Modeling and Optimization of Hybrid Fenton and Ultrasound Process for Crystal Violet Degradation Using AI Techniques. *Water* **2023**, *15*, 4274. [CrossRef]
29. Tahraoui, H.; Belhadj, A.-E.; Triki, Z.; Boudellal, N.R.; Seder, S.; Amrane, A.; Zhang, J.; Moula, N.; Tifoura, A.; Ferhat, R. Mixed Coagulant-Flocculant Optimization for Pharmaceutical Effluent Pretreatment Using Response Surface Methodology and Gaussian Process Regression. *Process Saf. Environ. Prot.* **2023**, *169*, 909–927. [CrossRef]
30. Tahraoui, H.; Belhadj, A.-E.; Amrane, A.; Houssein, E.H. Predicting the Concentration of Sulfate Using Machine Learning Methods. *Earth Sci. Inform.* **2022**, *15*, 1023–1044. [CrossRef]
31. Hamri, N.; Imessaoudene, A.; Hadadi, A.; Cheikh, S.; Boukerroui, A.; Bollinger, J.-C.; Amrane, A.; Tahraoui, H.; Tran, H.N.; Ezzat, A.O. Enhanced Adsorption Capacity of Methylene Blue Dye onto Kaolin through Acid Treatment: Batch Adsorption and Machine Learning Studies. *Water* **2024**, *16*, 243. [CrossRef]
32. Bouchelkia, N.; Tahraoui, H.; Amrane, A.; Belkacemi, H.; Bollinger, J.-C.; Bouzaza, A.; Zoukel, A.; Zhang, J.; Mouni, L. Jujube Stones Based Highly Efficient Activated Carbon for Methylene Blue Adsorption: Kinetics and Isotherms Modeling, Thermodynamics and Mechanism Study, Optimization via Response Surface Methodology and Machine Learning Approaches. *Process Saf. Environ. Prot.* **2023**, *170*, 513–535. [CrossRef]

33. Tahraoui, H.; Toumi, S.; Hassein-Bey, A.H.; Bousselma, A.; Sid, A.N.E.H.; Belhadj, A.-E.; Triki, Z.; Kebir, M.; Amrane, A.; Zhang, J. Advancing Water Quality Research: K-Nearest Neighbor Coupled with the Improved Grey Wolf Optimizer Algorithm Model Unveils New Possibilities for Dry Residue Prediction. *Water* **2023**, *15*, 2631. [CrossRef]
34. Zamouche, M.; Chermat, M.; Kermiche, Z.; Tahraoui, H.; Kebir, M.; Bollinger, J.-C.; Amrane, A.; Mouni, L. Predictive Model Based on K-Nearest Neighbor Coupled with the Gray Wolf Optimizer Algorithm (KNN_GWO) for Estimating the Amount of Phenol Adsorption on Powdered Activated Carbon. *Water* **2023**, *15*, 493. [CrossRef]
35. Aleboyeh, A.; Aleboyeh, H.; Moussa, Y. "Critical" Effect of Hydrogen Peroxide in Photochemical Oxidative Decolorization of Dyes: Acid Orange 8, Acid Blue 74 and Methyl Orange. *Dye. Pigment.* **2003**, *57*, 67–75. [CrossRef]
36. Changyin, Z.; Fengxiao, Z.; Fuwang, W.; Juan, G.; Guangping, F.; Dongmei, Z.; Guodong, F. Comparison of Persulfate Activation and Fenton Reaction in Remediating an Organophosphorus Pesticides-Polluted Soil. *Pedosphere* **2017**, *27*, 465–474.
37. Lemaire, J.; Laurent, F.; Leyval, C.; Schwartz, C.; Buès, M.; Simonnot, M.-O. PAH Oxidation in Aged and Spiked Soils Investigated by Column Experiments. *Chemosphere* **2013**, *91*, 406–414. [CrossRef]
38. Biache, C.; Lorgeoux, C.; Andriatsihoarana, S.; Colombano, S.; Faure, P. Effect of Pre-Heating on the Chemical Oxidation Efficiency: Implications for the PAH Availability Measurement in Contaminated Soils. *J. Hazard. Mater.* **2015**, *286*, 55–63. [CrossRef]
39. e Silva, P.T.D.S.; Da Silva, V.L.; de Barros Neto, B.; Simonnot, M.O. Phenanthrene and Pyrene Oxidation in Contaminated Soils Using Fenton's Reagent. *J. Hazard. Mater.* **2009**, *161*, 967–973. [CrossRef] [PubMed]
40. Rivas, F.J. Polycyclic Aromatic Hydrocarbons Sorbed on Soils: A Short Review of Chemical Oxidation Based Treatments. *J. Hazard. Mater.* **2006**, *138*, 234–251. [CrossRef] [PubMed]
41. Lemaire, J.; Buès, M.; Kabeche, T.; Hanna, K.; Simonnot, M.-O. Oxidant Selection to Treat an Aged PAH Contaminated Soil by in Situ Chemical Oxidation. *J. Environ. Chem. Eng.* **2013**, *1*, 1261–1268. [CrossRef]
42. Watts, R.J.; Stanton, P.C.; Howsawkeng, J.; Teel, A.L. Mineralization of a Sorbed Polycyclic Aromatic Hydrocarbon in Two Soils Using Catalyzed Hydrogen Peroxide. *Water Res.* **2002**, *36*, 4283–4292. [CrossRef] [PubMed]
43. Vicente, F.; Rosas, J.; Santos, A.; Romero, A. Improvement Soil Remediation by Using Stabilizers and Chelating Agents in a Fenton-like Process. *Chem. Eng. J.* **2011**, *172*, 689–697. [CrossRef]
44. Jung, Y.S.; Lim, W.T.; Park, J.; Kim, Y. Effect of pH on Fenton and Fenton-like Oxidation. *Environ. Technol.* **2009**, *30*, 183–190. [CrossRef] [PubMed]
45. Pignatello, J.J.; Oliveros, E.; MacKay, A. Advanced Oxidation Processes for Organic Contaminant Destruction Based on the Fenton Reaction and Related Chemistry. *Crit. Rev. Environ. Sci. Technol.* **2006**, *36*, 1–84. [CrossRef]
46. Sandford, S.A.; Bernstein, M.P.; Materese, C.K. The Infrared Spectra of Polycyclic Aromatic Hydrocarbons with Excess Peripheral H Atoms (Hn-PAHs) and Their Relation to the 3.4 and 6.9 Mm PAH Emission Features. *Astrophys. J. Suppl. Ser.* **2013**, *205*, 8. [CrossRef] [PubMed]
47. Maurya, A.; Singh, R.; Rastogi, S. Study of Vibrational Spectra of Polycyclic Aromatic Hydrocarbons with Phenyl Side Group. *J. Mol. Spectrosc.* **2023**, *391*, 111720. [CrossRef]
48. Obinaju, B.E.; Martin, F.L. ATR-FTIR Spectroscopy Reveals Polycyclic Aromatic Hydrocarbon Contamination despite Relatively Pristine Site Characteristics: Results of a Field Study in the Niger Delta. *Environ. Int.* **2016**, *89*, 93–101. [CrossRef]
49. Langhoff, S.R.; Bauschlicher, C.W.; Hudgins, D.M.; Sandford, S.A.; Allamandola, L.J. Infrared Spectra of Substituted Polycyclic Aromatic Hydrocarbons. *J. Phys. Chem. A* **1998**, *102*, 1632–1646. [CrossRef]
50. Karavoltsos, S.; Sakellari, A.; Bakeas, E.; Bekiaris, G.; Plavšić, M.; Proestos, C.; Zinelis, S.; Koukoulakis, K.; Diakos, I.; Dassenakis, M. Trace Elements, Polycyclic Aromatic Hydrocarbons, Mineral Composition, and FT-IR Characterization of Unrefined Sea and Rock Salts: Environmental Interactions. *Environ. Sci. Pollut. Res.* **2020**, *27*, 10857–10868. [CrossRef]
51. Tian, H.; Li, C.; Wang, Z.; Zhao, S.; Xu, Y.; Wang, S. Polycyclic Aromatic Hydrocarbons Degradation Mechanisms in Methods Using Activated Persulfate: Radical and Non-Radical Pathways. *Chem. Eng. J.* **2023**, *473*, 145319. [CrossRef]
52. Wang, J.; Zhang, X.; Zhou, X.; Waigi, M.G.; Gudda, F.O.; Zhang, C.; Ling, W. Promoted Oxidation of Polycyclic Aromatic Hydrocarbons in Soils by Dual Persulfate/Calcium Peroxide System. *Sci. Total Environ.* **2021**, *758*, 143680. [CrossRef] [PubMed]
53. Lin, M.; Ning, X.; An, T.; Zhang, J.; Chen, C.; Ke, Y.; Wang, Y.; Zhang, Y.; Sun, J.; Liu, J. Degradation of Polycyclic Aromatic Hydrocarbons (PAHs) in Textile Dyeing Sludge with Ultrasound and Fenton Processes: Effect of System Parameters and Synergistic Effect Study. *J. Hazard. Mater.* **2016**, *307*, 7–16. [CrossRef] [PubMed]